Multimodal binding of collybistin controls gephyrin filament formation in synaptic clustering

Nele Burdina[1], Filip Liebsch[1], Arthur Macha[1], Monika Gunkel[1], Elmar Behrmann[1]*, Guenter Schwarz[1,2]*

[1]Institute of Biochemistry, Department of Chemistry and Biochemistry, University of Cologne, 50674 Cologne, Germany

[2]Center for Molecular Medicine Cologne (CMMC), University of Cologne, Cologne, Germany

*Correspondence: Guenter Schwarz, gschwarz@uni-koeln.de, phone: +49 221 4709 6440; Elmar Behrmann, ebehrman@uni-koeln.de, phone: +49 221 470 76300

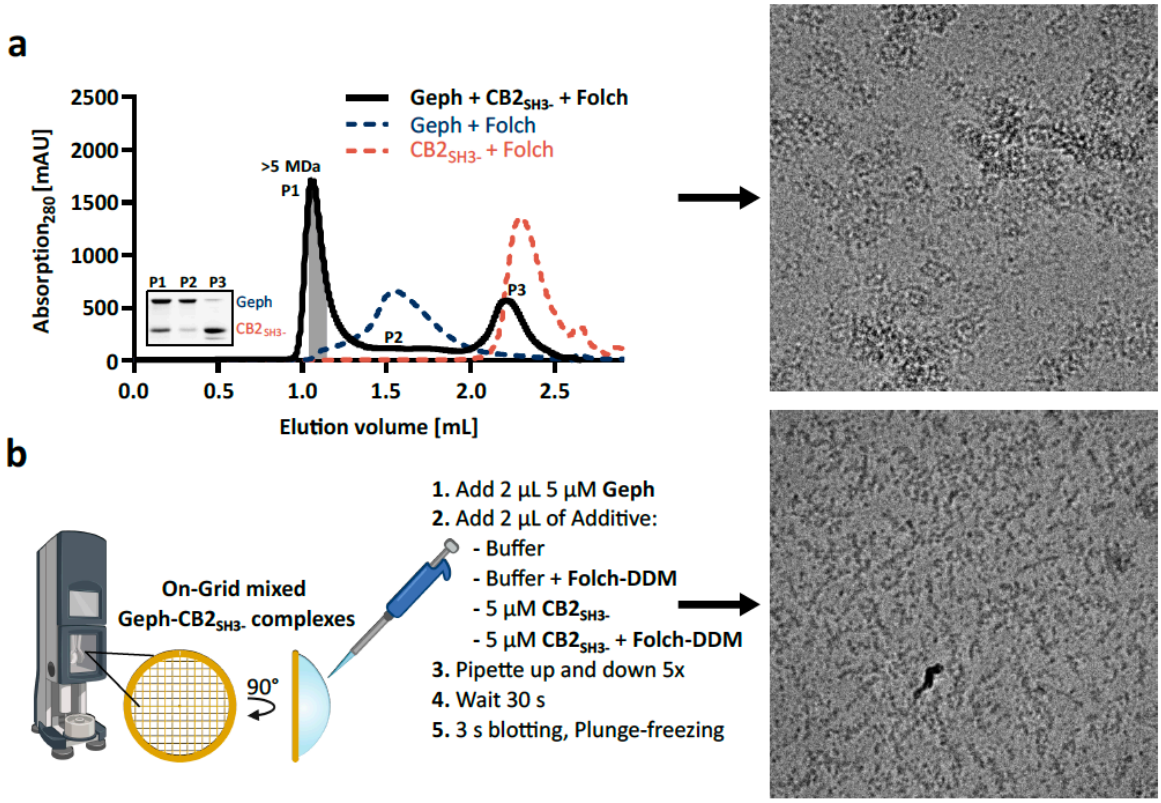

Extended Data Figure 1: Cryo-EM grid preparation of SEC purified and on-grid mixed Geph-CB complexes.

a, Cryo-EM grid preparation of the SEC-purified Geph-CB2$_{SH3-}$-Folch complex: Equimolar amounts of Geph and CB2$_{SH3-}$ together with Folch were applied onto a Superose 6 Increase 5/150 column, resulting in a high-molecular weight complex eluting at the column's cut-off (>5 MDa, black line). Single runs of Geph and CB2$_{SH3-}$ mixed with Folch are shown as a control (dotted lines). The inset depicts SDS-PAGE analysis of the peak fractions of the complex SEC run. The fraction corresponding to the Geph-CB2$_{SH3-}$-Folch complex was diluted to 2.5 µM and used for cryo-EM sample preparation, which resulted in large protein patches as shown by one representative micrograph. **b,** Scheme displaying the workflow for on-grid mixed Geph-CB2$_{SH3-}$(-Folch) complex cryo-EM sample preparation (created with BioRender.com). A representative micrograph of a sample containing Geph, CB2$_{SH3-}$ and Folch is shown, revealing isolated elongated particles suitable for single-particle cryo-EM analysis.

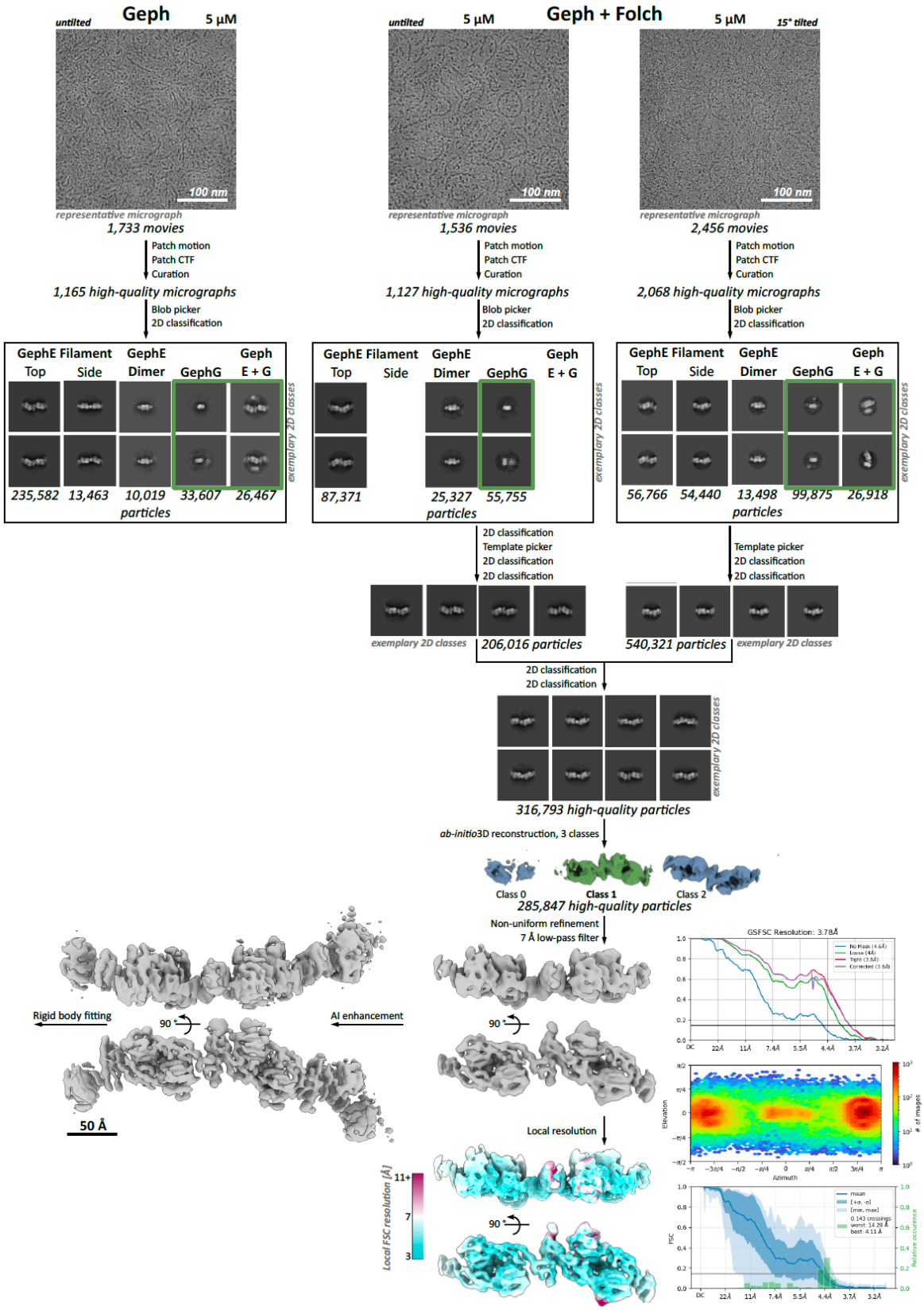

Extended Data Figure 2a: Overview of the single particle cryo-EM data processing workflow of Geph with and without Folch.

Data sets of cryo-EM samples of Geph mixed with only buffer (Geph) and Geph mixed with buffer containing Folch (Geph + Folch) were collected on a 300 kV cryo-electron microscope. An additional data set at a 15° tilt angle was recorded for Geph + Folch. Movies with low per-

frame drift rates, optimal CTF scores, and minimal astigmatism were selected for each data set. Particles were initially picked using a blob picker and subjected to unsupervised 2D classification. The resulting classes resembled the previously described GephE SDII-mediated filaments[1]. Untilted data sets predominantly showed top views of the putative GephE filament, while the tilted data acquisition yielded more side view particles. Additionally, classes resembling a specific viewing direction of GephG alone or in close proximity to GephE were observed (green boxes), consistent with previous cryo-EM studies of full-length Geph, suggesting high flexibility of GephC[1]. The quantification shown in Fig. 1c-f is based on particle numbers from GephE-containing classes, with representative examples of these classes displayed in the figure. Representative GephE filament classes were used as templates for particle picking in both untilted and tilted Geph + Folch data sets. The picked particles were curated using several rounds of 2D classification, selecting for particles resembling the GephE filament. Particles from both untilted and tilted data sets were then combined for ab-initio reconstruction. The green volume was used for further refinement in 3D using a non-uniform refinement algorithm, resulting in a map with a nominal resolution of 3.8 Å but which was anisotropic. The map was thus filtered to 7 Å before AI enhancement. The AI enhanced model was used for rigid body fitting.

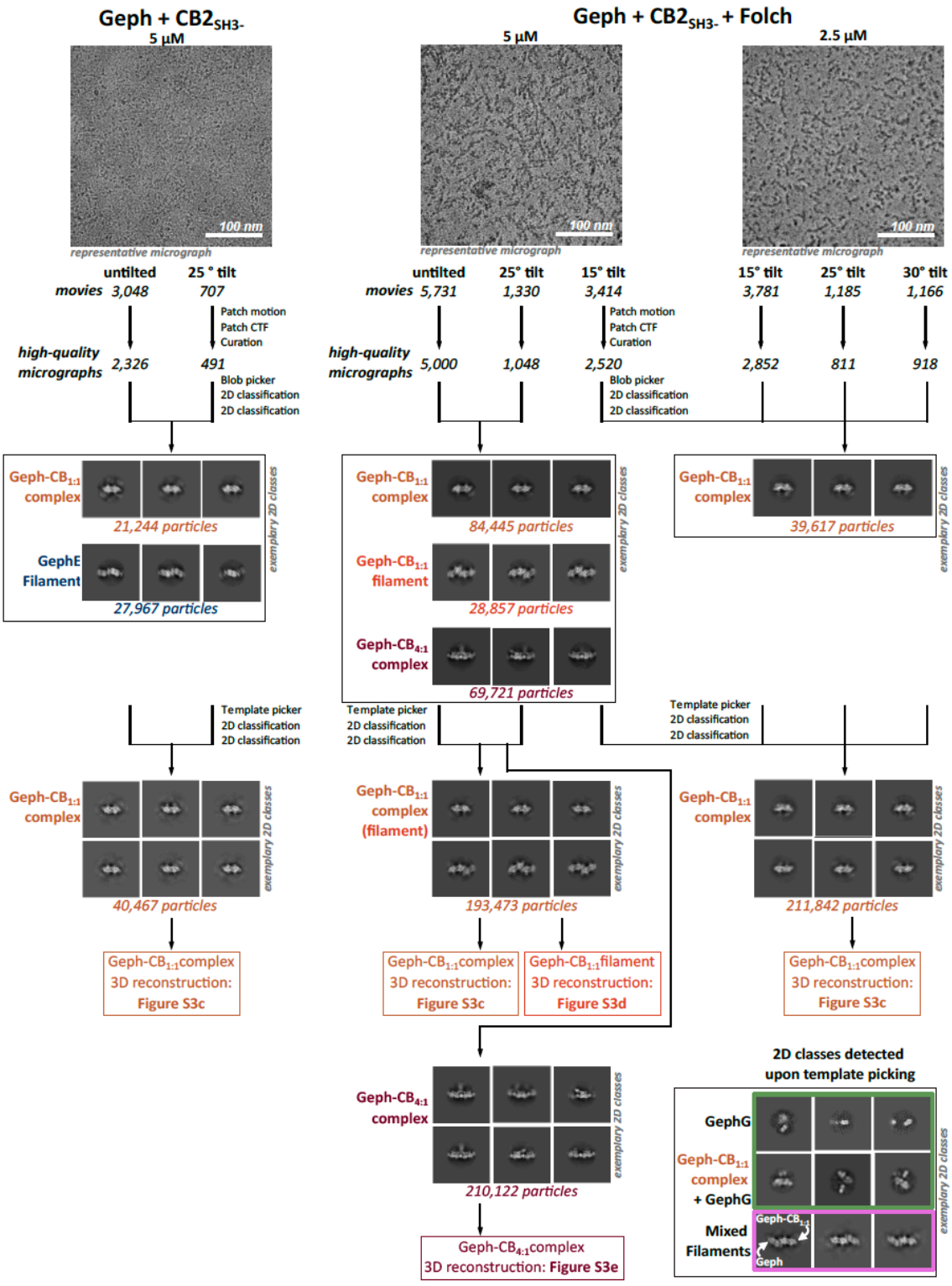

Extended Data Figure 2b: Overview of the single particle cryo-EM data processing workflow of Geph mixed with $CB2_{SH3-}$ with and without Folch.

Untilted as well as tilted data sets of cryo-EM samples of Geph mixed with $CB2_{SH3-}$ in the absence (Geph + $CB2_{SH3-}$) or presence of Folch (Geph + $CB2_{SH3-}$ + Folch) were collected on a 300 kV cryo-electron microscope. For Geph + $CB2_{SH3-}$ + Folch additional tilted data sets were recorded at a concentration of 2.5 µM. For each data set, movies with low per-frame drift rates, high CTF scores, and minimal astigmatism were selected. Particles were initially picked using a blob picker and subjected to unsupervised 2D classification. 2D classification of the

5 µM samples resulted in differently shaped 2D classes depending on the presence of Folch: Geph mixed with $CB2_{SH3}$- alone showed classes resembling the Geph-$CB_{1:1}$ complex and apo-GephE filaments. With the addition of Folch lipids, additionally Geph-$CB_{1:1}$ complex dimer/ filament classes as well as Geph-$CB_{4:1}$ complex classes were observed, while apo-GephE filaments were absent. The quantification shown in Fig. 1c-f is based on particle numbers from Geph-CB complex and apo-GephE classes, with representative examples of these classes also displayed in the figure. Notably, only one viewing direction was observed for all described classes. 2D classification of tilted datsets of Geph + $CB2_{SH3-}$ + Folch at a concentration of 2.5 µM resulted in tilted views of the Geph-$CB_{1:1}$ complex. Representative classes of the respective Geph-CB complexes were used as templates for particle picking in the corresponding data sets. Picked particles were curated using two rounds of 2D classification, selecting for particles resembling either the Geph-$CB_{1:1}$ or Geph-$CB_{4:1}$ complex. 2D classification after template picking revealed classes resembling GephG alone or in close contact to the Geph-$CB_{1:1}$ complex (green box), indicating a high flexibility of GephC. Furthermore, 2D classes resembling mixed filaments of one Geph-$CB_{1:1}$ complex forming a SDII-SDII´ interface with an apo-GephE dimer were detected (pink box).

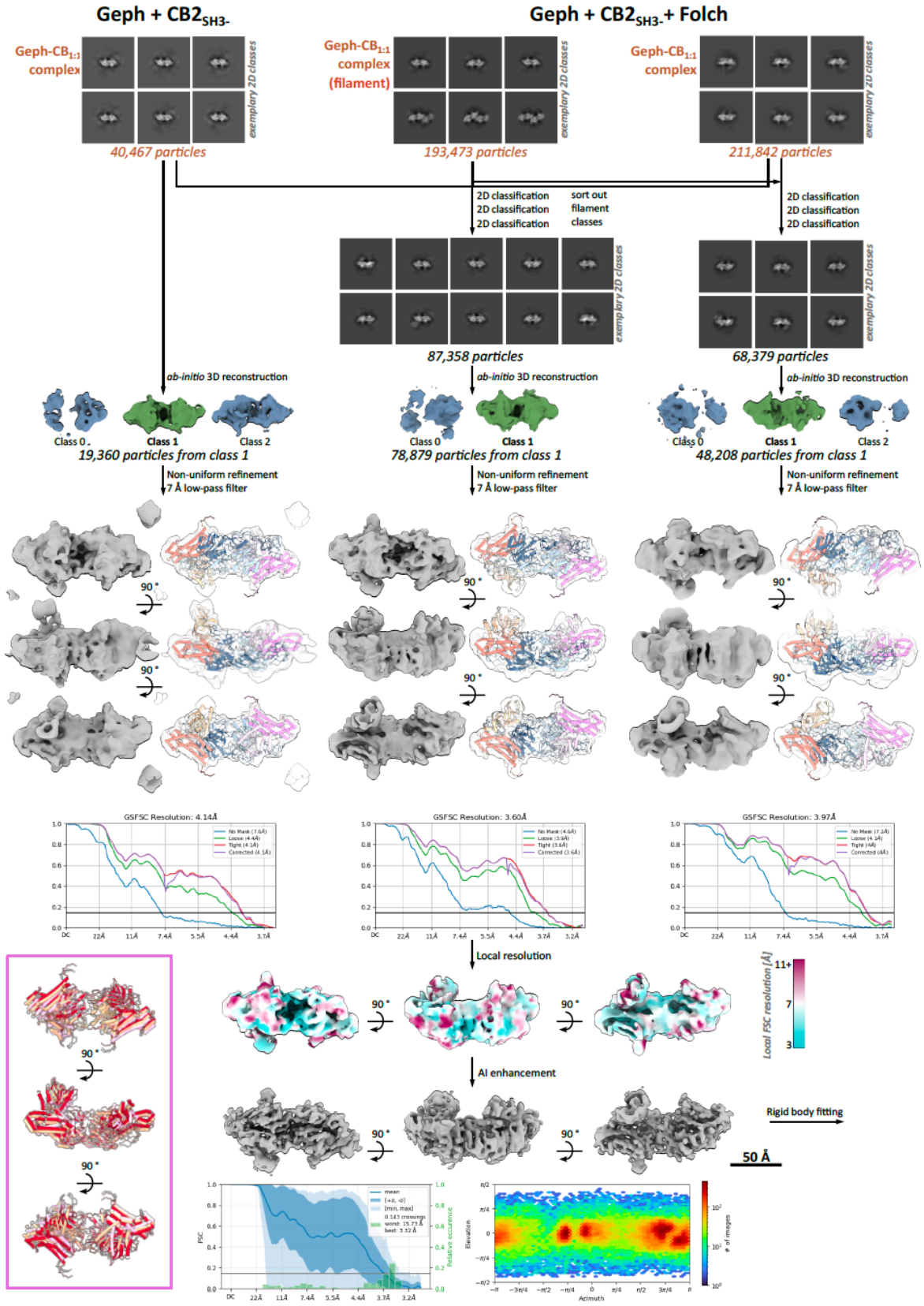

Extended Data Figure 2c: Overview of the single particle cryo-EM data processing workflow of the Geph-CB$_{1:1}$ complex.

Putative Geph-CB$_{1:1}$ complex particles from datasets of Geph mixed with CB2$_{SH3-}$ in the absence or presence of Folch lipids (described in Fig. S2b) were used for 3D reconstruction,

either independently or combined. Prior to 3D reconstruction, both the combined particle sets and the particles derived solely from the Geph + $CB2_{SH3-}$ + Folch sample were further curated by 2D classification selecting particles showing an isolated Geph-$CB_{1:1}$ complex while excluding complex dimer particles. For the 3D reconstruction, ab-initio reconstruction into two to three distinct classes was performed followed by a 3D refinement of the respective green volumes using a non-uniform refinement algorithm. Independent particle sets yielded maps with nominal resolutions of 4.2 Å and 4.0 Å while the combined particle set resulted in a map with a higher nominal resolution of 3.6 Å. Rigid body fitting for all three density maps resulted in a similar arrangement of two $CB2_{SH3-}$ bound to dimerized GephE (pink box: superposition of all three resulting structures). The map corresponding to the combined particle set yielded the best resolution and showed better-resolved structural features compared to the other two maps, and was thus used for further analysis. Due to the anisotropy of the map, it was filtered to 7 Å, AI enhanced and subsequently used for rigid body fitting.

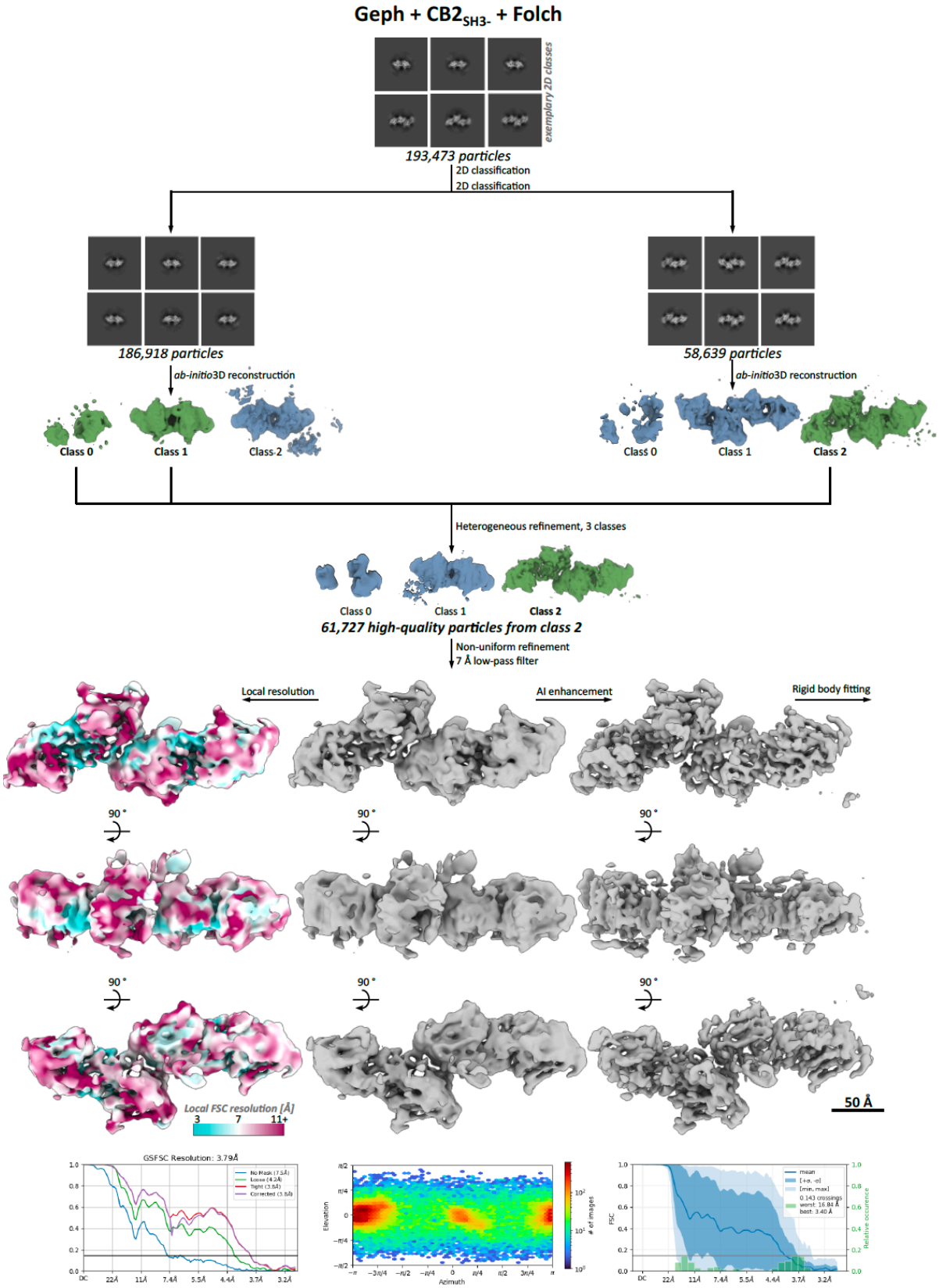

Extended Data Figure 2d: Overview of the single particle cryo-EM data processing workflow of the Geph-CB$_{1:1}$ complex dimer.

Putative Geph-CB$_{1:1}$ complex (monomer and dimer) particles from datasets of Geph mixed with CB2$_{SH3-}$ and Folch, as described in Fig. S2b, were subjected to further processing. The workflow consisted of the following steps: First two rounds of 2D classification were performed

to sort particles into classes showing either one (monomer) or two (dimer) Geph-$CB_{1:1}$ complexes. Curated particles were used for ab-initio reconstruction, sorting them into three distinct populations. The green volumes were used for a heterogenous refinement of all putative Geph-$CB_{1:1}$ complex (dimer) particles to separate isolated complexes (class 1) from complexes forming a dimer (class 2) as well as from junk particles (class 0). Particles contributing to the dimeric complex structure were refined in 3D using a non-uniform refinement algorithm, resulting in a map with a nominal resolution of 3.8 Å. Due to the anisotropy of the map, it was filtered to 7 Å, AI enhanced and afterwards used for rigid body fitting.

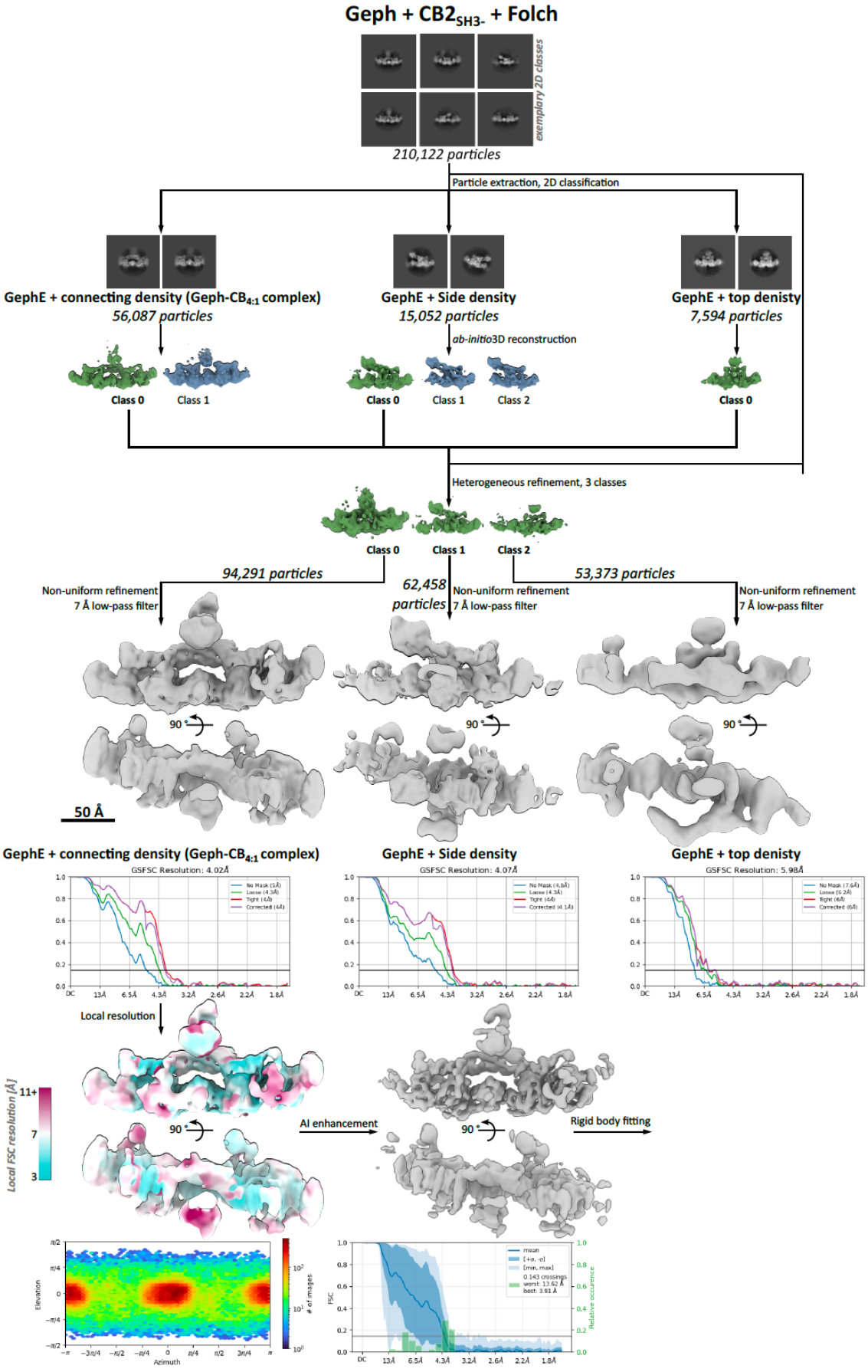
Geph + CB2SH3- + Folch
exemplary 2D classes
210,122 particles
Particle extraction, 2D classification
GephE + connecting density (Geph-CB4:1 complex)
56,087 particles
GephE + Side density
15,052 particles
GephE + top denisty
7,594 particles
ab-initio3D reconstruction
Class 0
Class 1
Class 2
Heterogeneous refinement, 3 classes
94,291 particles
62,458 particles
53,373 particles
Non-uniform refinement
7 Å low-pass filter
90 °
50 Å
GSFSC Resolution: 4.02Å
GSFSC Resolution: 4.07Å
GSFSC Resolution: 5.98Å
Local resolution
Local FSC resolution [Å]
11+
7
3
AI enhancement
Rigid body fitting
Elevation
Azimuth
# of images
FSC
Relative occurance

Extended Data Figure 2e: Overview of the single particle cryo-EM data processing workflow of the Geph-$CB_{4:1}$ complex.

Putative Geph-$CB_{4:1}$ complex particles derived from datasets of Geph mixed with $CB2_{SH3-}$ and Folch described in Fig. S2B underwent further processing. Further 2D classification revealed three different classes resembling different shapes: most particles correlate to classes showing a density connecting two GephE dimers (GephE + connecting density = Geph-$CB_{4:1}$ complex), while a minority of particles correlates to classes displaying a GephE dimer with additional density on one side (GephE + side density) or on top (GephE + top density) of the dimer interface. The respective particles were used for ab-initio reconstruction, sorting them into one to three distinct populations. The respective green ab initio volumes were used for heterogeneous refinement using all particles correlating to the three different classes. Particles correlating to each of the resulting volumes were individually refined in 3D using a non-uniform refinement algorithm, resulting in maps with nominal resolutions of 4.0 Å (GephE + connecting density = Geph-$CB_{4:1}$ complex), 4.1 Å (GephE + side density) and 6.0 Å (GephE + top density). The densities at the side and on top of GephE could not be identified due to the limited resolution, and thus these maps were not analyzed further. The density connecting two GephE dimers (Geph-$CB_{4:1}$ complex) resembles the shape of $CB2_{SH3-}$ and thus was used for rigid body fitting after lowpass filtering to 7 Å due to anisotropy as well as AI enhancement.

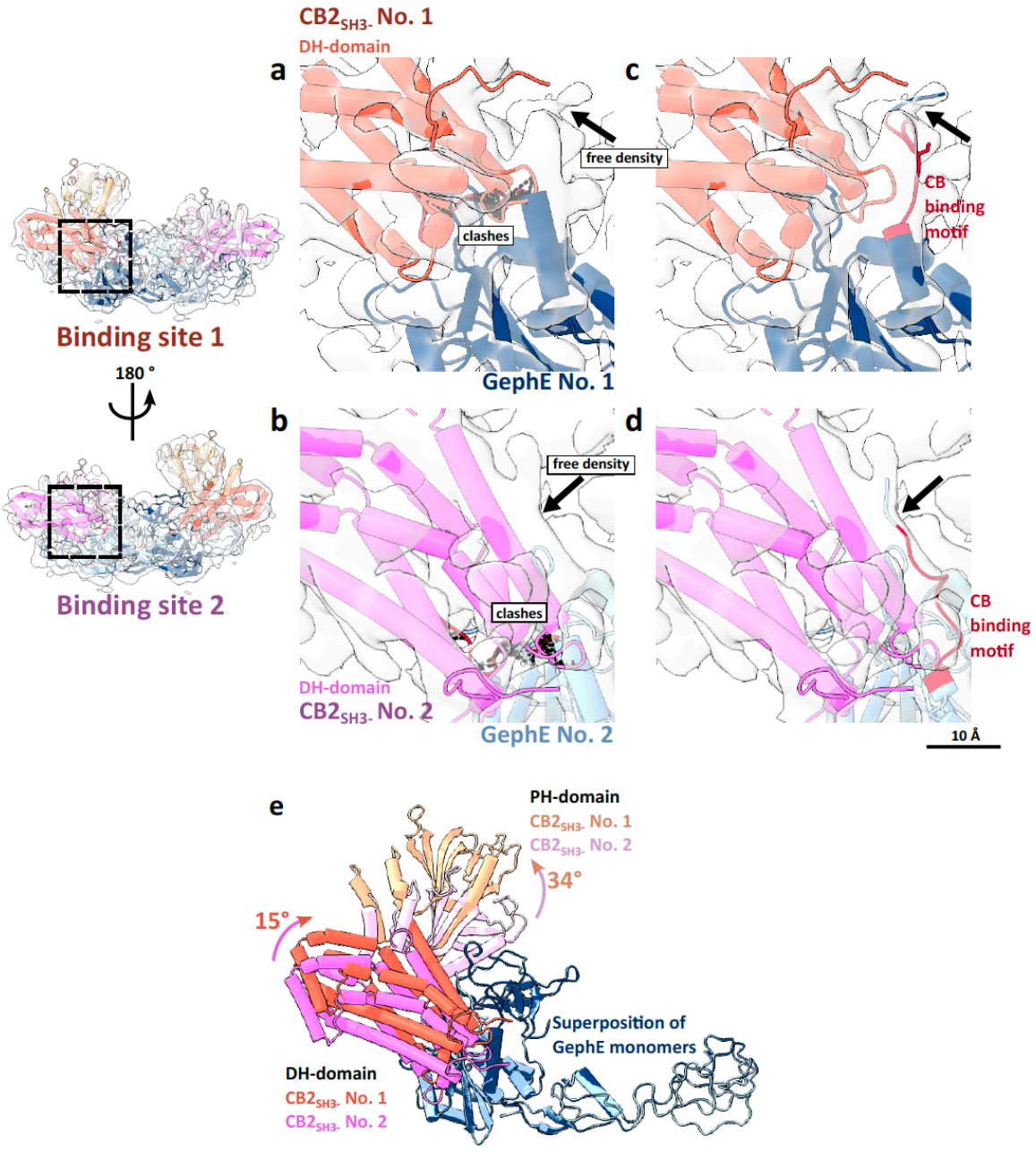

Extended Data Figure 3: Differential conformations of the CB-binding motif within the Geph-$CB_{1:1}$ complex.

a-d, Cartoon representation of the Geph-$CB_{1:1}$ complex according to the colouring in Fig. 1g with the CB binding motif $(320 – 29)^2$ colored in red, fitted into the corresponding cryo-EM density map depicted on the left. Zoomed-in views on the right display regions of binding sites 1 and 2. **a, b** The CB-binding motif results in clashes with the DH domain of $CB2_{SH3-}$ at both binding sites (black dotted lines) but free density adjacent to the binding motif could be observed in case of both binding sites. **c, d** The CB-binding motif was manually fitted into this density, releasing the clashes with $CB2_{SH3-}$ on both sites. **e,** Superposition according to the GephE monomers of the Geph-$CB_{1:1}$ complex, showing structural differences between the two binding sites. The DH domain between the two binding sites is rotated by 15°, while the PH domain is rotated by 34°, showing that the two binding sites of the Geph-$CB_{1:1}$ are not symmetrical.

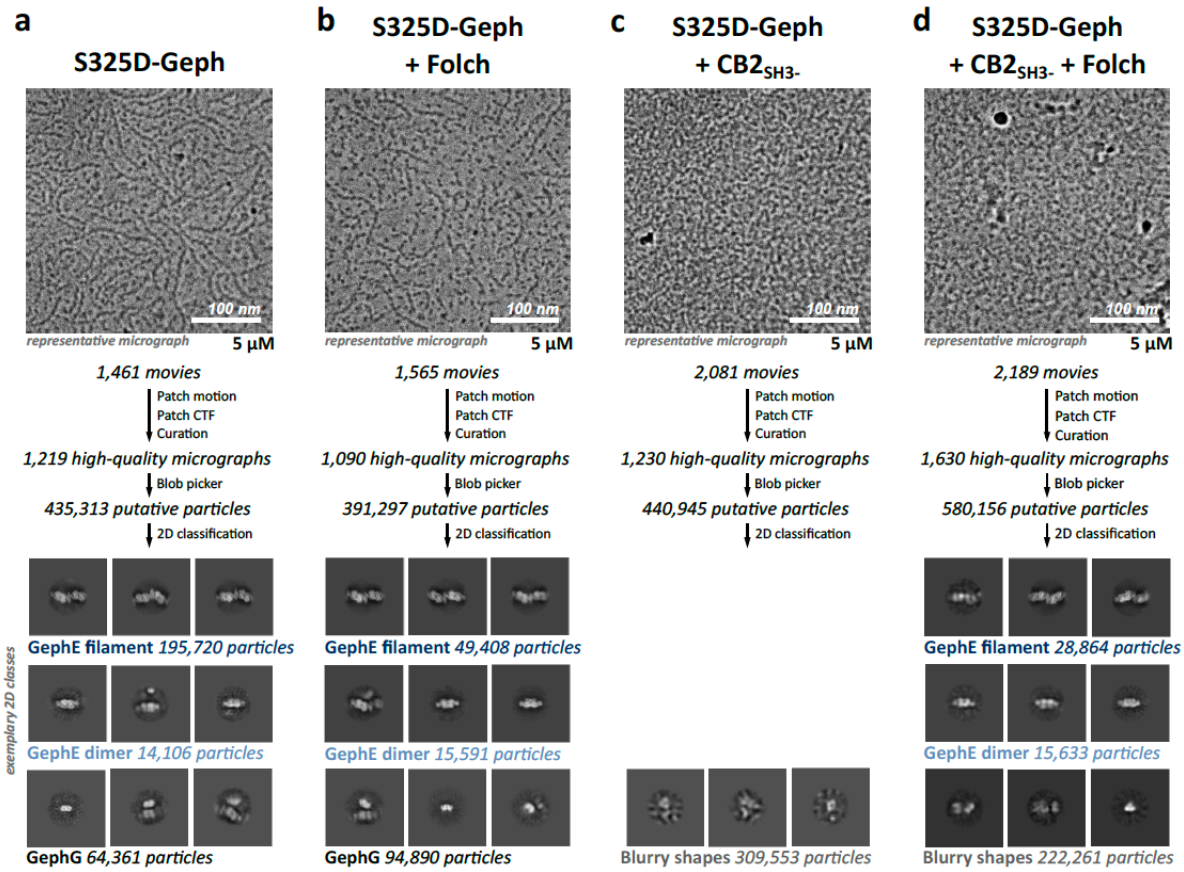

Extended Data Figure 4: Single particle cryo-EM data processing workflow of S325D-Geph alone and mixed with $CB2_{SH3-}$ and/or Folch.

Data sets of S325D-Geph **a,** alone **b,** mixed with Folch **c,** mixed with $CB2_{SH3-}$ or **d,** mixed with $CB2_{SH3-}$ and Folch, respectively, were collected on a 300 kV cryo-electron microscope. Movies were selected for low per-frame drift rates, good CTF scores and low astigmatism. Particles were picked using a blob picker, and then subjected to unsupervised 2D classification, resulting in different classes depending on the the presence of $CB2_{SH3-}$. **a, b,** The respective classes resulting from data sets without $CB2_{SH3-}$ were resembling GephE filaments, isolated GephE dimers as well as GephG. **c, d,** 2D classes resulting from data sets with $CB2_{SH3-}$ resembled GephE filaments, isolated GephE dimers as well as blurry shapes, but no classes resembling Geph-CB complexes were detected. In the WT Geph-$CB_{1:1}$ complex, Ser325 is in close contact to the $CB2_{SH3-}$ DH-domain (Fig. 2c) suggesting that a negative charge at this position introduced by the phosphomimic mutant might disrupt the interaction with $CB2_{SH3-}$. Conversely, in the Geph-$CB_{4:1}$ complex, Ser325 is not in close proximity to $CB2_{SH3-}$ (Fig. 4a). The negative charge of the phosphate group could either cause conformational changes abolishing Geph-$CB_{4:1}$ complex formation or the Geph-$CB_{1:1}$ complex might be a prerequisite for Geph-$CB_{4:1}$ complex formation.

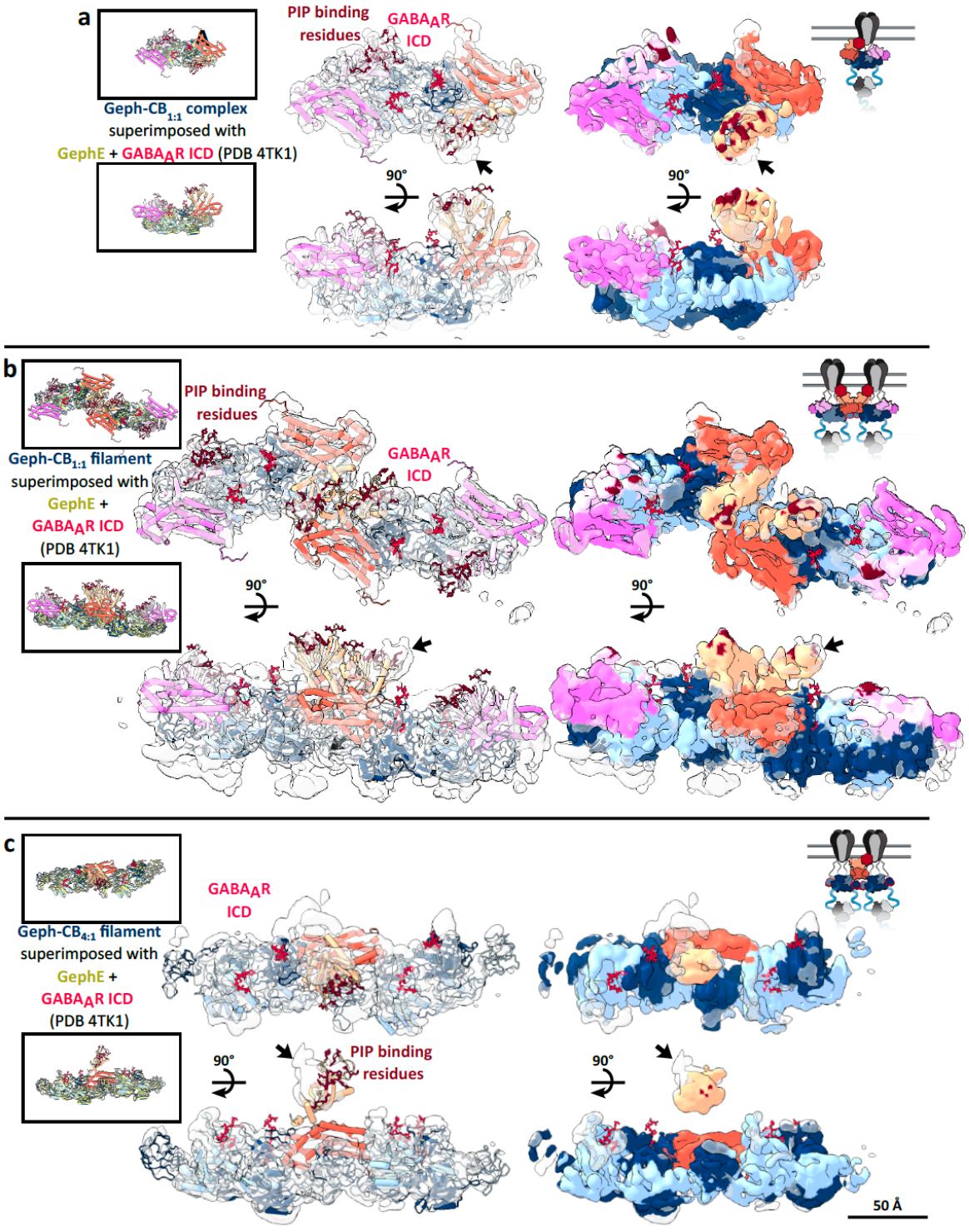

Extended Data Figure 5: PIP and receptor binding sites are accessible and point into the same direction in the different Geph-CB complexes.

The position of the GABA$_A$R α3 core binding motif (light red) as well as the PIP binding sites (dark red) are highlighted in the structural models/ maps of **a,** the Geph-CB$_{1:1}$ complex **b,** the Geph-CB$_{1:1}$ complex dimer and **c,** the Geph-CB$_{4:1}$ complex: The left panel depicts a superposition of the respective Geph-CB complexes (cartoon representation) with the crystal structure of dimerized GephE (yellow, cartoon representation) in complex with a GABA$_A$R α3 core binding motif derived peptide (light red, stick representation, PDB 4TK1[3]). Additionally, PIP-binding residues within the CB PH-domain determined within docking and molecular

dynamic simulations studies[4] are shown in the stick representation (dark red). The middle panel shows the Geph-CB complexes (cartoon representation) fitted into the respective cryo-EM density maps, with superimposed $GABA_AR$ α3 binding peptide (light red, stick) and highlighted PIP-binding residues (dark red, stick). The right panel shows the cryo-EM density maps of the Geph-CB complexes coloured according to the respective Geph and $CB2_{SH3-}$ domains (as in Fig. 1g) and PIP-binding regions are coloured dark red. The superimposed $GABA_AR$ α3 binding peptide is shown in light red in the stick representation. The receptor binding peptide does not overlap with any of the complex densities, indicating that the receptor binding pocket remains accessible upon $CB2_{SH3-}$ binding. Similarly, the PIP-binding sites are surface-exposed in all Geph-CB complexes, suggesting that these sites remain available for interaction for all complex configurations. The receptor and PIP binding sites point into the same direction for all Geph-CB complexes, indicating that simultaneous receptor and PIP binding at postsynaptic membranes is possible as depicted by the cartoon shown on the right (created with BioRender.com). Additional density can be observed in close proximity to PIP-binding sites (indicated by black arrows) of 'open' $CB2_{SH3-}$ (colored in orange) and is absent in case of 'closed' $CB2_{SH3-}$ (colored in pink). This additional density could correlate either with bound lipids or with increased flexibility of 'open' $CB2_{SH3-}$.

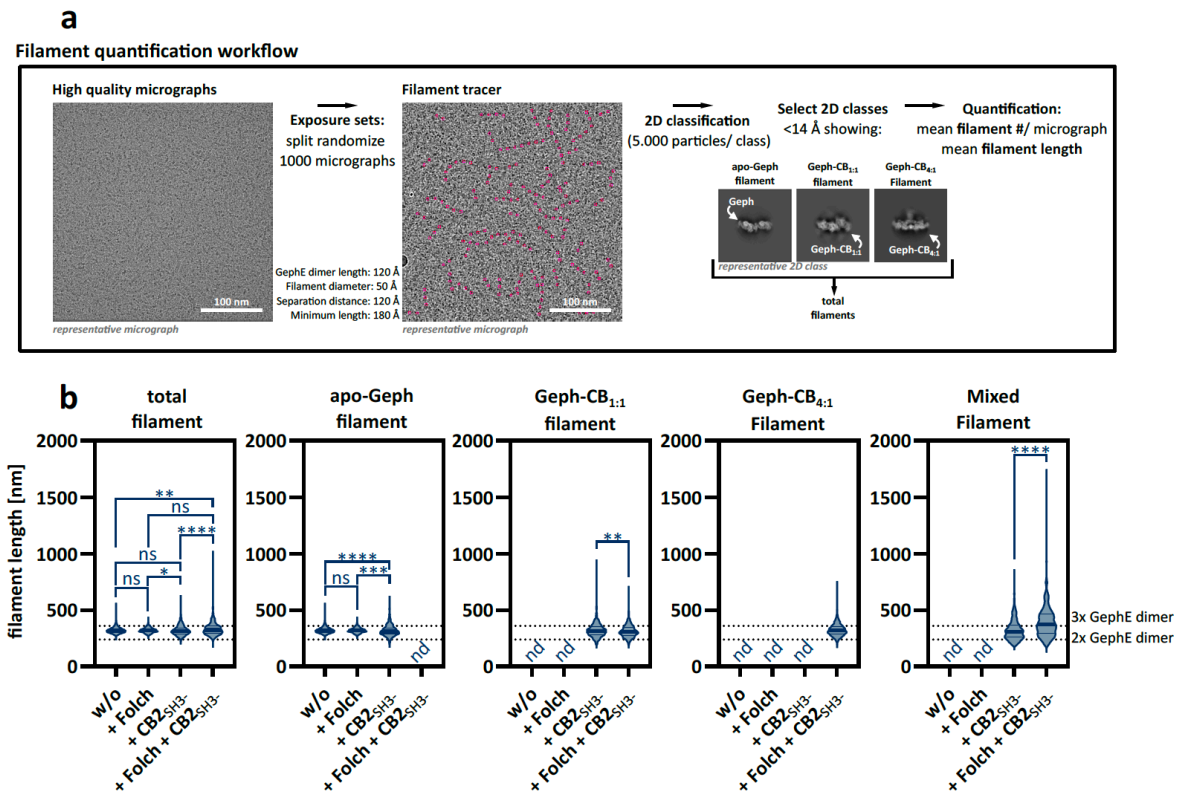

196

197

198 **Extended Data Figure 6: Filament quantification workflow, determining the mean length**
199 **and number of Geph filaments per micrograph.**

200 **a,** Workflow for the quantification of the mean filament number (shown in Fig. 5 a-e) and length
201 per micrograph: Putative filaments were identified using a dedicated filament tracer of a
202 random subset of 1000 micrographs of the respective datasets correlating to samples of Geph
203 mixed with only buffer (w/o) or $CB2_{SH3-}$ in the absence or presence of Folch. The putative
204 filament particles were curated by unsupervised 2D classification. Filaments containing
205 particles with resolutions better than 14 Å were categorized as either apo-Geph (CB-free),
206 Geph-$CB_{1:1}$ complex or Geph-$CB_{4:1}$ complex filaments, based on classification results.
207 Filaments identified to contain particles from more than one category were classified as mixed
208 filaments. **b,** Quantification of the mean filament length per micrograph for Geph mixed with
209 only buffer (w/o) or $CB2_{SH3-}$ in the presence or absence of Folch. The average length of the
210 detected filaments across all samples ranged between 315 and 328 nm, corresponding to two
211 to three GephE dimers per filament (240 – 360 nm, indicated by dotted lines), as the filament
212 tracer tool tends to recognize filament fragments rather than full-length filaments due to the
213 flexibility of the SDII-filament interface described previously[1]. The length of filaments between
214 the respective conditions was tested for significance using a Kruskal-Wallis followed by Dunn's
215 post-hoc test (apo-Geph: $H = 24.88$, $p < 0.0001$; n = 1000 micrographs) and two-tailed Mann-
216 Whitney test (Geph-$CB_{1:1}$: $U = 446{,}717$, $p = 0.003$; mixed: $U = 101{,}865$, $p < 0.0001$; n = 1000
217 micrographs). Statistical significance is designated as $*p \leq 0.05$, $**p \leq 0.01$, $***p \leq 0.001$ and
218 $****p \leq 0.0001$.

219

References

1. Macha, A. *et al.* Gephyrin filaments represent the molecular architecture of inhibitory postsynaptic densities.

2. Harvey, K. *et al.* The GDP-GTP exchange factor collybistin: An essential determinant of neuronal gephyrin clustering. *Journal of Neuroscience* **24**, 5816–5826 (2004).

3. Maric, H. M. *et al.* Molecular basis of the alternative recruitment of GABAA versus glycine receptors through gephyrin. *Nat Commun* **5**, 5767 (2014).

4. Chiou, T. T. *et al.* Mutation p.R356Q in the collybistin phosphoinositide binding site is associated with mild intellectual disability. *Front Mol Neurosci* **12**, (2019).